

Simulating Natural Ventilation in and Around Buildings by Fast Fluid Dynamics

Mingang Jin¹, Wangda Zuo², Qingyan Chen¹

¹*School of Mechanical Engineering, Purdue University, West Lafayette, IN 47906, USA*

²*Department of Civil, Architectural, and Environmental Engineering, University of Miami, Coral Gables, FL 33124, USA*

Qingyan Chen (Corresponding Author)

Email: yanchen@purdue.edu

Phone: +1-765-496-7562

Fax: +1-765-494-0539

ABSTRACT

Natural ventilation is a sustainable technology that can provide a well-built environment and also save energy. The application of natural ventilation to buildings requires a careful approach in the early design phase, and fast, simple design tools are greatly needed. Fast fluid dynamics (FFD) can provide useful airflow information at a speed much faster than CFD so that it is a potential design tool for natural ventilation. This study thus validated FFD with test cases representing different types of natural ventilation. The results showed that FFD was capable of predicting the main air flow feature and ventilation rate with reasonable accuracy for wind-driven or buoyancy-driven natural ventilation. FFD simulation can reflect the influence of wind direction and surrounding buildings on natural ventilation.

Keywords: Natural ventilation; Fast fluid dynamics; Computational fluid dynamics

NOMENCLATURE

F_i	body force
i, j	index of coordinate
P	pressure
S	source term
t	time
U_i, U_j	velocity components in x_i and x_j directions, respectively
U^n, U^{n+1}	velocity at previous and current time step, respectively
U^*, U^{**}	intermediate velocity
x_i, x_j	spatial coordinates in i and j direction, respectively
Δt	time step size

Γ	transport coefficient
ρ	density
ν	kinetic viscosity
Φ	scalar in transport equation

1. Introduction

Natural ventilation is a sustainable building technology that can provide a good indoor environment and save energy [1]. It is preferred over mechanical ventilation for sustainable building design. However, the design of natural ventilation is more difficult than that for mechanical ventilation because the driving force of natural ventilation is complicated [2] and its performance is highly dependent on various factors, such as outdoor microclimate, building shape and orientation, window location and orientation, and internal heat sources [3]. These factors should be thoroughly considered at the early stage of building design in order to achieve good natural ventilation. A design tool that can predict the influence of these factors on natural ventilation will be necessary for architects to optimize the natural ventilation design.

Many methods have been developed to predict natural ventilation, such as analytical and empirical models for single-sided or cross natural ventilation with simple geometry. Warren et al. [4] derived an analytical expression for buoyancy-driven, single-sided natural ventilation and an empirical expression for wind-driven, single-sided natural ventilation. Phaff et al. [5] developed an empirical correlation that could account for both wind and buoyancy effects. For cross ventilation, CIBSE [6] proposed analytical expressions separately for wind-driven and buoyancy-driven cross ventilation of a single zone building with two openings on each side. Li et al. [7] also developed an analytical model for single-zone buildings with two openings, including wind-driven, stack-driven and combined-driven flows. With simple equations, the analytical and empirical expressions developed in the literature are easy to apply and quick to compute, but they are only suitable for simple or single-zone buildings.

For buildings with multiple rooms, multi-zone models [8] have been proposed to predict the natural ventilation rate through the buildings. With the assumption of uniform temperature and pressure in a single room, the multi-zone model treats rooms in the building as a set of zones connected by airflow paths. Solving the flow equations together with the mass conservation allows the airflow rate and pressure in each zone to be computed efficiently. There are many applications of multi-zone models for studying natural ventilation. For example, Eriksson et al. [9] applied a multi-zone model to evaluate natural ventilation in a Swedish school building. Emmerich et al. [10] simulated the performance of natural and hybrid ventilation systems in an office building with a multi-zone model. However, due to the well mixed assumption and neglect of the momentum effect, the multi-zone model may not be accurate for predicting airflows with a strong temperature gradient or with a strong momentum effect in a zone [11]. Also, this model cannot provide air velocity or resolve airflow patterns or temperature distributions within a zone, which are very important for analyzing the indoor air quality and thermal comfort.

Through numerically solving a set of partial differential equations for the conservation of mass, momentum, and energy, computational fluid dynamics (CFD) can provide the distributed air velocity and temperature within zones. It has been successfully used for analyzing the performance of natural ventilation. Tantasavasdi et al. [12] used the CFD to explore the possibility of natural ventilation in houses in Thailand. Norton et al. [13] applied the CFD to model and design natural ventilation system in the agricultural industry. Chen et al. [14] also

presented several examples of designing natural ventilation using the CFD. Due to its large demand for computation, running the CFD analysis is time consuming and is mainly used for final design evaluation and research projects. For early stages of building design, much iterations are usually required to optimize the design, so it would be impractical for architects to evaluate the performance of each natural ventilation design by using CFD. Thus, an ideal approach for early design should be able to provide rich airflow information in and around buildings as the CFD does, and should be as efficient as the multi-zone model.

As an intermediate approach between the multi-zone model and CFD, fast fluid dynamics (FFD) can provide fast simulation of airflow in buildings [15]. Thus, it has the potential for natural ventilation design. Zuo et al. [15], [16] developed a two-dimensional FFD for airflow simulations in buildings and found that FFD could offer rich airflow information for buildings with reasonable accuracy and faster speed compared with CFD. Jin et al. [17] further extended FFD for three dimensional flows in a building. Their results showed that FFD could successfully capture the three dimensionality of the airflow and provide reliable simulations for indoor airflows at a speed about 15 times faster than CFD. However, FFD has not been applied to simulating natural ventilation, so it is necessary to evaluate its performance for the current application. This forms the basis of the current investigation as reported in this paper.

2. Research method

2.1 Fast fluid dynamics

Fast fluid dynamics was originally developed by Stam [18] for computer graphics, simulating efficiently incompressible fluid flows. Zuo et al. [15], [19] introduced and improved the algorithm of FFD for simulating airflow in buildings. To achieve high computational efficiency, FFD applies a three-step time-advancement scheme to solve the Navier-Stokes and continuity equations for incompressible viscous fluid:

$$\frac{\partial U_i}{\partial t} + U_j \frac{\partial U_i}{\partial x_j} = -\frac{1}{\rho} \frac{\partial p}{\partial x_i} + \nu \frac{\partial^2 U_i}{\partial x_j \partial x_j} + \frac{1}{\rho} F_i, \quad (1)$$

$$\frac{\partial U_i}{\partial x_i} = 0, \quad (2)$$

where $i, j = 1, 2, 3$. U_i is the i th component of the velocity vector, p pressure, ρ density, F_i i th component of body forces, and x_i i th component of spatial coordinates, respectively.

The three-step time-advancement scheme splits the Navier-Stokes equations into three discretized equations:

$$\frac{U_i^* - U_i^n}{\Delta t} = -U_j^n \frac{\partial U_i^n}{\partial x_j}, \quad (3)$$

$$\frac{U_i^{**} - U_i^*}{\Delta t} = \nu \frac{\partial^2 U_i^{**}}{\partial x_j \partial x_j} + \frac{1}{\rho} F_i, \quad (4)$$

$$\frac{U_i^{n+1}-U_i^{**}}{\Delta t} = -\frac{1}{\rho} \frac{\partial p}{\partial x_i}, \quad (5)$$

where U^n and U^{n+1} represent the velocity at the previous and current time step, respectively, and U^* and U^{**} are the intermediate velocity obtained from solving Eqs. (3) and (4), respectively. FFD first solves Eq. (3) explicitly for advection by using a first-order semi-Lagrangian method [20]. By applying the Lagrangian advection on the Eulerian grid, the semi-Lagrangian method can achieve enhanced stability at larger time steps. To solve U^* in Eq. (3), FFD uses backward trajectory to determine the departure locations of particles arriving at the grid cells at the end of each time step. The velocity at the grid cells can then be updated with the velocity at the departure point, which can be interpolated from the velocity at surrounding grid cells. U^* can be expressed by the following equation:

$$U_i^*(x_j) = U_i^n(x_j - \Delta t U_j^n), \quad (6)$$

where $U_i^*(x_j)$ is U_i^* at location $x_j = (x_1, x_2, x_3)$. Thereafter, FFD solves the diffusion equation with a source term by a fully implicit scheme to obtain another intermediate velocity, U^{**} . Finally the pressure projection is conducted to project the intermediate velocity field into a space of divergence free vector field to obtain pressure and updated velocity. By substituting Eq. (2) into Eq. (5), the following Poisson equation can be derived:

$$\frac{\partial^2 p}{\partial x_j \partial x_j} = \frac{\rho}{\Delta t} \frac{\partial U_i^{**}}{\partial x_i}. \quad (7)$$

By solving Eq. (7) for pressure, FFD updates the velocity field with Eq. (5) to obtain U^{n+1} . After obtaining the velocity field, transport equations for other scalars can be further solved in a similar manner:

$$\frac{\partial \Phi}{\partial t} + U_j \frac{\partial \Phi}{\partial x_j} = \Gamma \frac{\partial^2 \Phi}{\partial x_j \partial x_j} + S, \quad (8)$$

where Φ is the scalar to be solved, Γ the transport coefficient, and S the source term, respectively.

Although FFD solves the Navier-Stokes equation as CFD does, the computing speed is more important for FFD than for CFD. The semi-Lagrangian method that is applied for solving the advection equation allows FFD to adopt larger time steps, so the simulation by FFD can advance much faster than that by CFD. FFD also uses simple and lower order schemes to improve computational efficiency. For example, it uses linear interpolation instead of higher-order interpolation in the semi-Lagrangian method. The pressure projection also uses only the first-order projection. FFD further increases its computing speed by reducing the iterations for solving the coupled momentum and continuity equations. In FFD, to obtain a more converged solution for satisfying both momentum and continuity equations inner iterations are not applied for each time step as in CFD. As a result, FFD has a lower computing cost but less accuracy than CFD.

Because accuracy is not the objective of FFD, FFD maintains its simplicity without integrating any turbulence models in the current study. Instead, a previous study showed that the lower order scheme applied in FFD can generate high numerical viscosity [19], which can be used as a substitute for turbulent viscosity. Numerical viscosity is dependent on grid size and will decrease

when the grid is refined.

2.2 Boundary conditions

In FFD, paired boundary conditions for both velocity and pressure are required to solve implicit diffusion equations and the Poisson equation. This study applied three typical flow boundary types: inlet, outlet, and solid wall. At the inlet boundary, a Dirichlet boundary condition was applied for velocity. In addition, FFD used the physical velocity boundary condition as a boundary condition for intermediate velocity as follows:

$$U_i^{**} = U_i^{n+1} = U_{\text{inlet}} , \quad (9)$$

where U_{inlet} is the given velocity at the inlet. The Neumann boundary condition for pressure was derived from Eqs. (5) and (7):

$$\frac{\partial p}{\partial n} \Big|_b = 0 , \quad (10)$$

where n represents the local normal to the studied surface. At the outlet, FFD applied local mass conservation for the outflow boundary for velocity as suggested by Li et al. [21]. Similarly, Neumann boundary conditions can be derived for pressure at outflow boundaries as shown by Eq. (10).

This investigation applied no-slip wall boundary conditions for the solid wall. The air velocity at a solid wall boundary is zero, as shown by Eq. (11):

$$U_i^{**} = U_i^{n+1} = U_{\text{wall}} = 0 , \quad (11)$$

where U_{wall} is the air velocity at the wall. Also, Eq. (10) was applied as boundary condition for the pressure.

3. Results and discussion

First, this investigation applied FFD to two test cases representing different types of natural ventilation: wind-driven, single-sided, and cross ventilation in a wind tunnel, and buoyancy-driven, single-sided ventilation in a full-scale chamber. The computed distributions of the air temperature and velocity by FFD were compared with corresponding experimental data to evaluate the performance of FFD for simulating natural ventilation. FFD was then used to simulate wind-driven, natural ventilation through a four-zone, full-scale building in a wind tunnel, which is a more complicated case. The ventilation rate under different wind directions was computed by FFD and compared with the experimental data. The study further applied FFD to simulate ventilation rate by cross ventilation for Building 661 in Navy Yard, Philadelphia, which presented a practical application. The performance of FFD was evaluated for predicting the impact of the surrounding buildings on the natural ventilation design. The test cases are summarized in Table 1.

In this study, the FFD simulation results were also compared with those predicted by the CFD. For the FFD simulations, grid independence was examined separately for each test case. Using a finer grid could improve the accuracy, but it reduced the speed. Since FFD is designed for fast flow simulation and a coarse grid is always preferred in its application, this paper reported only

the results obtained using coarse grids.

3.1 Wind-driven, single-sided, and cross ventilation in a wind tunnel

The first case study is a wind-driven, natural ventilation case based on the experiment conducted by Jiang et al. [22]. The experiment employed a scaled building model with openings and a wind tunnel. Three different types of wind-driven, natural ventilation were studied: single-sided ventilation with a windward opening, single-sided ventilation with a leeward opening, and cross ventilation with openings in both windward and leeward walls.

The building model is depicted in Figure 1. It has two openings of the same size on opposite walls. One of the openings was blocked when studying single-sided ventilation with leeward opening or windward opening. The model dimensions were $250\text{ mm} \times 250\text{ mm} \times 250\text{ mm}$ for the building and $84\text{ mm} \times 125\text{ mm}$ for the opening. The vertical distribution of mean velocity at the inlet of the wind tunnel followed a logarithmic law, and the Reynolds number based on the inflow velocity at the building height was 1.4×10^5 . The experiment measured the mean velocity distribution along ten vertical lines in the streamwise direction, and their locations are shown in Figure 2.

Figure 3 compares the velocity distribution in the middle section by FFD and the experiment for the three cases. At the windward side of the building model, the airflow fields predicted by FFD agreed well with the measurement data for all three cases. Downstream, FFD could also predict the recirculation zone for all three cases with some discrepancies. However, FFD was not able to simulate flow separation above the building model, which was observed by the experiment. Further study showed that FFD could only capture the separation zone with a finer mesh. For the airflow in the building, both the experiment and the FFD results showed low velocity distribution for single-sided ventilation. For cross ventilation, FFD also predicted the circulation at the upper part of the building model as shown by the experiment (Figure 3(c)). Overall, FFD could capture the major pattern of the airflow.

This study further compared the velocity profiles along the streamwise locations, as shown in Figure 4. The results computed by FFD were also compared with the CFD results by Alloca [23] for the three cases. On the upstream side of the building ($X = -H/25$), the velocity profiles predicted by CFD agreed very well with the experimental data in all three cases. FFD also computed velocity profiles close to the experimental data with some discrepancies at $Z=0.25$. For the velocity distribution in the building model ($X = H/2$), both FFD and CFD predicted low velocity in the building for single-sided ventilation. For cross ventilation, FFD could predict the velocity variation in the building, but the agreement was poorer than CFD. Also, at the top of the building, FFD was not able to capture the recirculation (negative velocity around $Z=0.25$) as CFD did. At the region near the leeward wall ($X = H+H/25$), the results simulated by CFD and FFD agreed well with the experimental data. However, downstream from the building model ($X = H+H/2$), neither CFD nor FFD could not obtain accurate simulation results for the three cases. Alloca [23] also made a similar conclusion, that CFD with the RANS turbulence model could not predict the velocity distribution well for the wake region behind the building model. Jiang [24] found that only LES can achieve an accurate prediction. Through the comparison above, this study found that FFD could predict the main airflow distribution for wind-driven, single-sided, and cross natural ventilation with a lower accuracy than CFD with turbulence models.

3.2 Buoyancy-driven, single-sided natural ventilation

To validate the performance of FFD for buoyancy-driven, natural ventilation, this investigation used the experimental case by Jiang et al. [25]. The experiment used a test chamber in a laboratory to simulate the indoor environment and the laboratory space to simulate the outdoor environment. A 1500 W baseboard heater was placed in the test chamber to generate buoyancy force. The door was open to simulate buoyancy-driven, single-sided ventilation. Figure 5(a) shows the layout of the chamber and the laboratory. In the experiment, the air velocity and temperature distributions were measured at five different locations as shown in Figure 5(b).

Because the walls of the test chamber had high thermal resistance, they were considered to be adiabatic. The surface temperatures of the laboratory were measured and used as thermal boundary conditions for our study, as shown in Table 2.

Figure 6 compares the airflow field simulated by FFD and CFD [24]. The flow pattern predicted by FFD was in good agreement with that predicted by CFD. Both FFD and CFD predicted the high speed regions along the top and bottom parts of the room, and the plume above the heat source. FFD can also predict the secondary recirculation at the upper right corner of the chamber that was observed in the experiment by Jiang et al. [25]. Although the simulated flow pattern outside the door was slightly different between FFD and CFD, FFD captured the main airflow features of single-sided natural ventilation just as CFD did.

Figure 7 compares the velocity profiles computed by FFD and CFD with the corresponding experimental data. In the chamber, the velocity profiles computed by FFD and CFD showed acceptable agreement with the data. Both FFD and CFD predicted high velocity near the ceiling and the floor and low velocity at the middle height inside the chamber. For the airflow outside the door (Position P1), neither FFD nor CFD could predict the velocity variation over the door with high accuracy. FFD and CFD showed similar accuracy for predicting airflow distribution for the buoyancy-driven natural ventilation.

Table 3 compares the air change rates computed by FFD and CFD [24] with the experimental data. Both FFD and CFD provided reasonable estimates for air change rates induced by buoyancy-driven natural ventilation, and FFD performed rather well in this case.

For the temperature distribution in the chamber, Figure 8 compares the computed temperature profiles by FFD and CFD with the experimental data at the five measurement positions. The thermal stratification was clearly predicted by both FFD and CFD. Although FFD predicted a higher temperature at the ceiling level, the temperature distribution simulated by FFD was in reasonable agreement with the experimental data. Also, the largest thermal stratification computed by FFD occurred in the middle section of the room, which was consistent with the experimental data and the CFD simulation by Jiang [24].

3.3 Cross ventilation through a four-zone building model

This study further tested FFD for prediction of the impact of wind direction on natural ventilation. Sawachi et al. [26] measured discharge coefficients at the building openings under different wind directions using a full-scale building model in a large wind tunnel. The tested model was a full-scale building model with dimensions of 5.53 m \times 5.53 m \times 3.0 m, and it was divided into four sub-zones of the same size. As shown in Figure 9, the building had two openings with a size of 0.86 m \times 1.74 m each, located on opposite walls. The full-scale building model can be rotated in

the wind tunnel to study the impact of different wind directions on cross ventilation. This study applied FFD to simulate the airflow path through the building model and the ventilation rate under cross ventilation with different wind directions.

Figure 10 depicts the airflow pattern on a horizontal plane at the middle height (1.2 m above the floor) in the building model when the wind direction is normal to the opening A (0 degree). The experimental data in Figure 10(a) showed that most air flowed from opening A through Path C due to the preserved momentum of the incoming wind. Then the air passed through opening D and flowed out through opening E. Additionally, because of the existence of partitions, the airflow was separated, and circulations formed in the room. The FFD results in Figure 10(b) showed a very similar trend of flow pattern but with some discrepancies in the recirculation details, which is still acceptable.

The wind direction would change the pressure difference of the two openings and thus influence the ventilation rate through the building. Design tools should be able to predict the impact of wind direction on ventilation rate. Figure 11 compares the ventilation rate computed by FFD with the corresponding measured data. The ventilation rate was highest when the wind direction was normal to the opening A, and lowest when the wind direction was parallel to opening A. FFD could predict this trend and the calculated ventilation rate showed reasonable agreement with the experimental result. Thus, FFD was capable of predicting the impact of wind direction on natural ventilation.

3.4 Natural ventilation through a building complex

Site planning is one of the important factors that influence the performance of natural ventilation. Surrounding buildings may provide shelter from the wind or increase the wind exposure due to channel effects that would significantly affect natural ventilation. It is essential that a design tool predict the impact of surrounding buildings on the natural ventilation of the building concerned. This study applied FFD to simulate wind-driven cross-ventilation for Building 661 at Navy Yard, Philadelphia, which will serve as the headquarters of the Energy-Efficient Building Hub. Figure 12 shows a model of Building 661 and its surroundings. The tall buildings around Building 661 may block the wind from the southwest direction, which would affect the building's natural ventilation. The prevailing wind direction in Philadelphia is southwest with an average speed of 4 m/s.

This study simulated the airflow distribution around and inside Building 661 for natural ventilation with prevailing wind direction by FFD and CFD using ANSYS Fluent [27]. Figure 13 compares the velocity contour computed by FFD and CFD. Upstream, FFD predicted a similar velocity distribution as CFD. Both programs can capture the high speed region around the southwest corner of Building 661. But on the downstream side, noticeable discrepancies between FFD and CFD were found. This was consistent with our findings in previous test cases which showed that FFD could not accurately predict the velocity distribution in the wake region behind the buildings.

This study also compared the ventilation rate through Building 661 computed by FFD and CFD. Although the computed ventilation rates were not exactly the same, they were still in the same order of magnitude. Thus, FFD can be used for a complex flow such as this.

It should be noted that the FFD simulation had difficulty in achieving mass conservation for this case. Because FFD used here a fixed number of Gauss-Seidel iterations to solve the projection equation, it was not capable of solving the equation to sufficient precision. Thus, the mass

conservation was not satisfied for every cell in this case. Although it is possible to increase the number of iterations, this would significantly reduce the computational efficiency of FFD, which contradicts our objective. Applying a high-efficiency solver for solving projection equations or applying coarse grid projection would be preferable for improving FFD. This is a topic for future research.

4. Conclusions

This study investigated FFD performance for simulating natural ventilation. FFD was applied to different types of natural ventilation, such as wind-driven, single-sided natural ventilation, wind-driven cross natural ventilation, and buoyancy-driven, single-sided natural ventilation. This study also examined the impact of wind direction and applied FFD to natural ventilation in a building complex.

For wind-driven, single-sided natural ventilation and cross natural ventilation, FFD can accurately predict the velocity distribution on the upstream side of a building. However, FFD was not as accurate as CFD with a RANS model for simulating airflow distribution inside and on the downstream side of the building. Nevertheless, FFD can still capture the main airflow feature.

For buoyancy-driven, single-sided natural ventilation, FFD can predict the airflow pattern in the room generated by a heat source as well as thermal stratification in the room. The air change rate calculated by FFD also agreed well with the experimental data.

FFD can determine the impact of wind direction on cross natural ventilation. The ventilation rate computed under different wind directions agreed reasonably well with the corresponding experimental data.

The application of FFD for simulating natural ventilation in a building complex demonstrated that FFD is capable of predicting the influence of the surrounding buildings on natural ventilation. However, the FFD simulation could not achieve mass conservation without excessive computing effort.

Acknowledgement

This work was supported by the U.S. Department of Energy through the Energy-Efficiency Building Hub program led by Pennsylvania State University.

References

- [1] Q. Chen, Using computational tools to factor wind into architectural environment design, *Energy and Buildings*, vol. 36, pp. 1197–1209, 2004.
- [2] P. F. Linden, The Fluid Mechanics of Natural Ventilation, *Annual Review of Fluid Mechanics*, vol. 31, no. 1, pp. 201–238, Jan. 1999.
- [3] S. J. Emmerich, W. S. Dols, and J. W. Axley, *Natural ventilation review and plan for design and analysis tools*. National Institute of Standards and Technology, 2001.
- [4] P. Warren, Ventilation through openings on one wall only, in *Energy conservation in heating, cooling, and ventilating buildings*, Dubrovnik, Yugoslavia, 1977.

- [5] H. Phaff and W. De Gids, Ventilation rates and energy consumption due to open windows: a brief overview of research in the Netherlands, *Air Infiltration Review*, vol. 4, no. 1, pp. 4–5, 1982.
- [6] CIBSE, Design data, in *CIBSE Guid-Volum A*, Chartered Institution of Building Service Engineers, 1986.
- [7] Y. Li and A. Delsante, On natural ventilation of a building with two openings, *Document-AIR INFILTRATION CENTRE AIC PROC*, no. 19, pp. 188–196, 1998.
- [8] J. Axley, S. Emmerich, and S. Dols, An approach to the design of natural and hybrid ventilation systems for cooling buildings, presented at the Indoor Air, Monterey, USA, 2002.
- [9] J. Eriksson and A. Wahlstrom, Use of Multizone Air Exchange Simulation to Evaluate a Hybrid Ventilation System, *Transactions- American Society of Heating Refrigerating and Air-conditioning Engineers*, vol. 108, pp. 811–817, 2002.
- [10] S. J. Emmerich, Simulated Performance of Natural and Hybrid Ventilation Systems in an Office Building, *International Journal of Heating Ventilation Air-conditioning and Refrigerating Research*, vol. 12, no. 4, pp. 975–1004, 2006.
- [11] L. (Leon) Wang and Q. Chen, Evaluation of some assumptions used in multizone airflow network models, *Building and Environment*, vol. 43, no. 10, pp. 1671–1677, Oct. 2008.
- [12] C. Tantasavasdi, J. Srebric, and Q. Chen, Natural ventilation design for houses in Thailand, *ENERGY AND BUILDINGS*, vol. 33, no. 8, pp. 815–824, 2001.
- [13] T. Norton, J. Grant, R. Fallon, and D.-W. Sun, Assessing the ventilation effectiveness of naturally ventilated livestock buildings under wind dominated conditions using computational fluid dynamics, *Biosystems Engineering*, vol. 103, no. 1, pp. 78–99, May 2009.
- [14] L. R. Glicksman and J. Lin, *Sustainable urban housing in China principles and case studies for low-energy design*. Dordrecht: Springer, 2006.
- [15] W. Zuo and Q. Chen, Real buildings, *Indoor Air*, vol. 19, no. 1, pp. 33–44, Feb. 2009. -time or faster- than -
- [16] W. Zuo and Q. Chen, Fast and informative flow simulations in a building by using fast fluid dynamics model on graphics processing unit, *Building and Environment*, vol. 45, no. 3, pp. 747–757, Mar. 2010.
- [17] M. Jin, W. Zuo, and Q. Chen, Validation of three dimensional fast fluid dynamics for indoor airflow simulations, in *Proceedings of 2nd International Conference on Energy and Environment*, Boulder, Colorado, 2012.
- [18] J. Stam, Stable fluids, in *The 26th annual conference on Computer graphics and interactive techniques*, Los Angeles, 1999, pp. 121–128.
- [19] W. Zuo, J. Hu, and Q. Chen, Improvements in FFD Modeling by Using Different Numerical Schemes, *Numerical Heat Transfer, Part B: Fundamentals*, vol. 58, no. 1, pp. 1–16, Aug. 2010.
- [20] A. Staniforth and J. Côté, Semi-Lagrangian Integration Schemes for Atmospheric Models—A Review, *Monthly Weather Review*, vol. 119, no. 9, pp. 2206–2223, Sep. 1991.
- [21] P. W. Li and W. Q. Tao, Effects of outflow boundary condition on convective heat transfer with strong recirculating flow, *Heat and Mass Transfer*, vol. 29, pp. 463–470, Sep. 1994.
- [22] Y. Jiang, D. Alexander, H. Jenkins, R. Arthur, and Q. Chen, Natural ventilation in buildings: measurement in a wind tunnel and numerical simulation with large-eddy simulation, *Journal of Wind Engineering and Industrial Aerodynamics*, vol. 91, no. 3, pp. 331–353, 2003.
- [23] C. Allocca, Single-sided natural ventilation : design analysis and general guidelines, Massachusetts Institute of Technology, [Cambridge, Mass.], 2001.
- [24] Y. Jiang, Study of natural ventilation in buildings with large eddy simulation, Massachusetts Institute of Technology, 2002.

- [25] Y. Jiang and Q. Chen, Buoyancy-driven single-sided natural ventilation in buildings with large openings, *International Journal of heat and mass transfer.*, vol. 46, no. 6, pp. 973–988, 2003.
- [26] T. Sawachi, K. Narita, N. Kiyota, H. Seto, S. Nishizawa, and Y. Ishikawa, Wind pressure and airflow in a full-scale building model under cross ventilation, *The International Journal of Ventilation*, vol. 2, no. 4, pp. 343–358, 2004.
- [27] ANSYS, ANSYS FLUENT 12.1 Documentation, ANSYS Inc., PA.

Table 1. Summary of test cases

Case	Scale	Data Compared	References
Wind-driven, single-sided and cross ventilation	Small-scale wind tunnel	Temperature and velocity	Experiment by Jiang et al.[22] , CFD by Allocca [23]
Buoyancy driven, single-sided natural ventilation	Full-scale chamber	Temperature, velocity, and ventilation rate	Experiment by Jiang et al. [25], CFD by Jiang [24]
Cross ventilation through a four-zone building model	Full-scale wind tunnel	Velocity and ventilation rate	Experiment by Sawachi et al. [26]
Building 661	Two story building	Velocity and ventilation rate	CFD

Table 2. Surface temperatures of the laboratory

	Ceiling	Floor	North wall	South wall	East wall	West wall
Surface temperature (°C)	23.11	22.11	23.01	22.90	20.94	22.83

Table 3 Air change rates for single-side natural ventilation

	Experimental measurements	CFD	FFD
Air change rate (ACH)	9.18-12.6	15.2	9.36

Caption of figures

Figure 1. Schematic view of the building model for wind-driven, single-sided, and cross ventilation (Jiang et al.[22])

Figure 2. The positions for the velocity measurement in the streamwise mid-section (Jiang et al. [22])

Figure 3. Comparison of velocity field in the streamwise mid-section computed by FFD and the experiment for (a) single sided, windward ventilation, (b) single sided, leeward ventilation, and (c) cross ventilation

Figure 4. Mean velocity distributions in the streamwise direction for (a) single-sided, windward ventilation, (b) single-sided, leeward ventilation, and (c) cross ventilation

Figure 5. Sketch of (a) the layout of the laboratory and (b) measurement positions

Figure 6. Comparison of airflow patterns simulated by (a) FFD and (b) CFD by Jiang et al.[25]

Figure 7. Comparison of the computed velocity profiles with the experimental data at the five measurement positions

Figure 8. Comparison of the computed temperature profiles with the experimental data at the five measurement positions

Figure 9. Sketch of the four-zone building model

Figure 10. Comparison of airflow patterns (a) observed in experiment by Sawachi et al. [26] and (b) simulated by FFD

Figure 11. Comparison of ventilation rates with different wind angles by FFD and the data from Sawachi et al. [26]

Figure 12. Sketch of Building 661 and its surrounding

Figure 13. Comparison of velocity distribution simulated by (a) CFD and (b) FFD

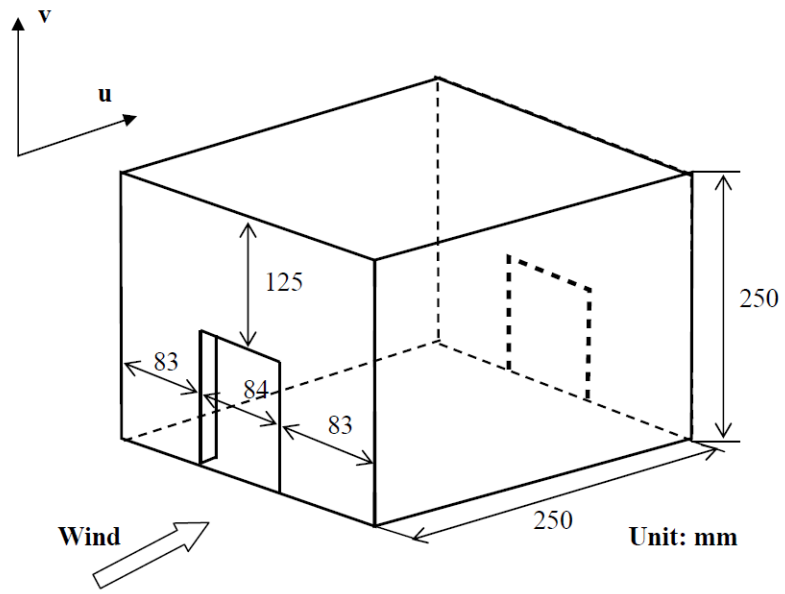


Figure 1

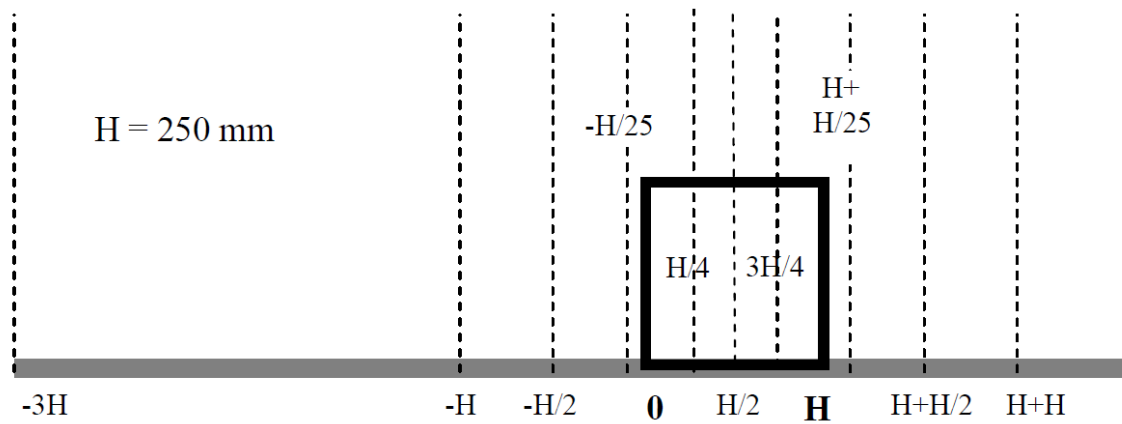
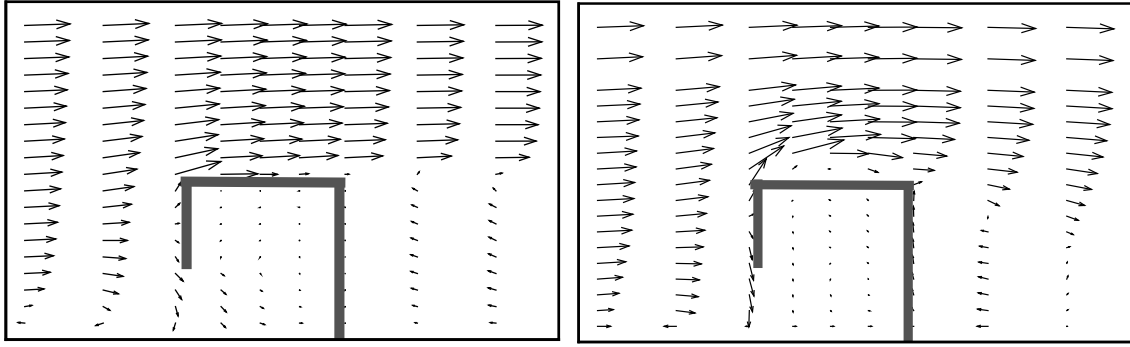


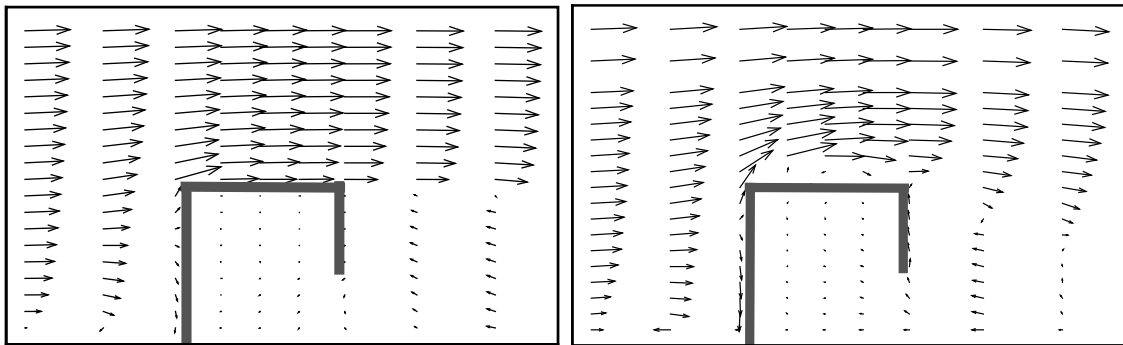
Figure 2



FFD

Measurement

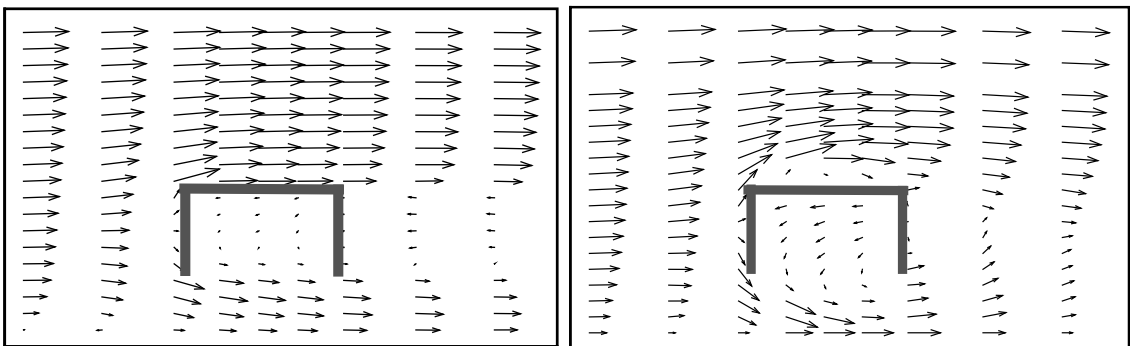
(a)



FFD

Measurement

(b)



FFD

Measurement

(c)

Figure 3

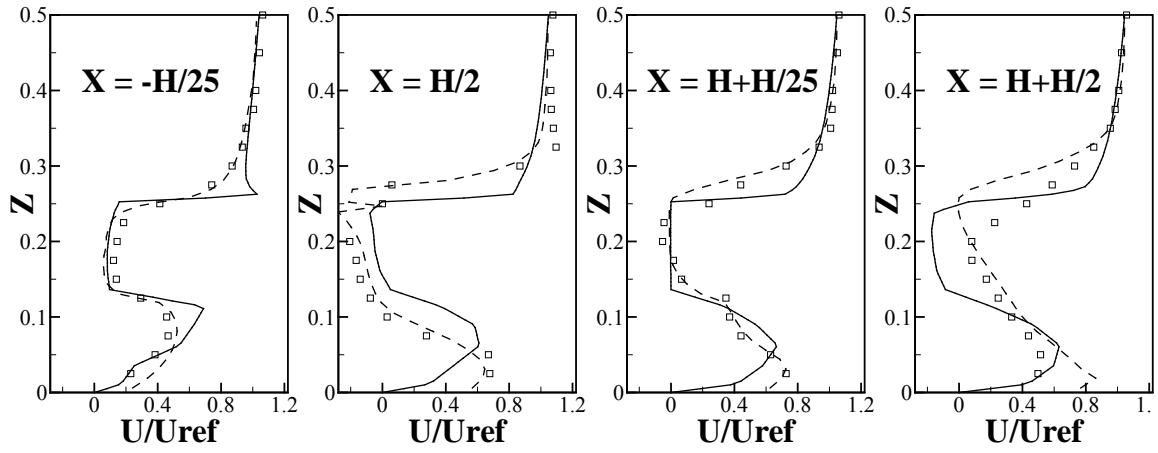
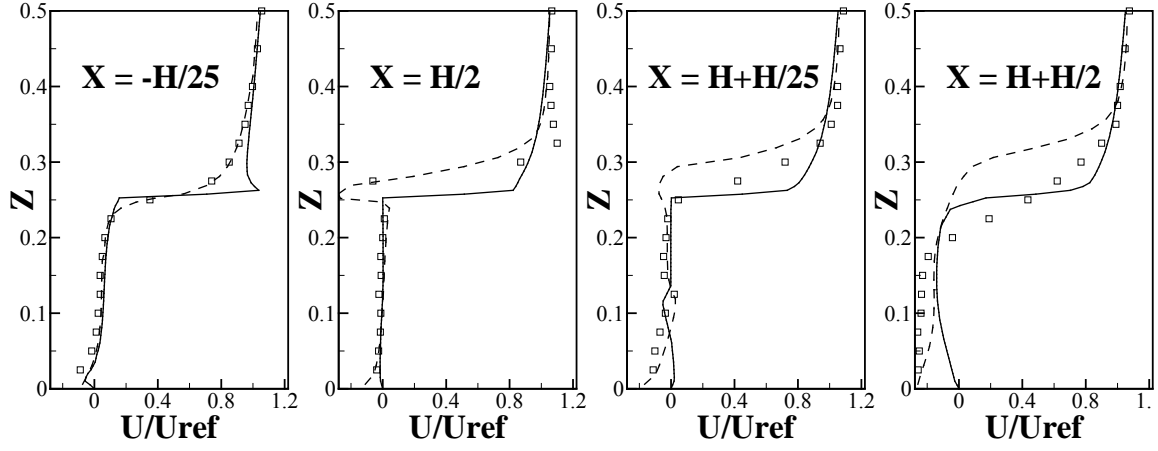
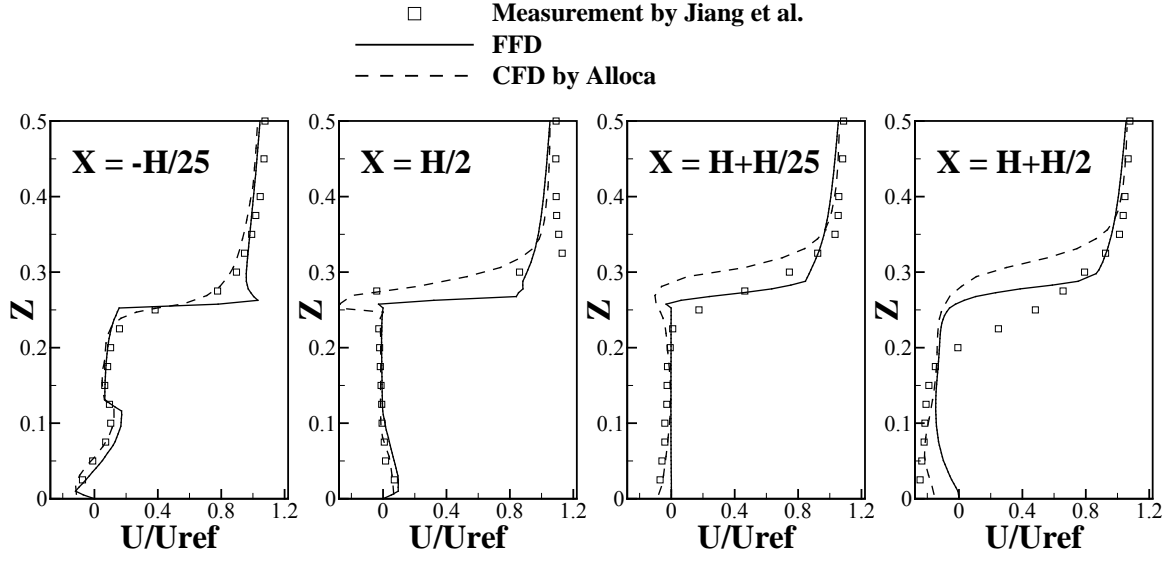


Figure 4

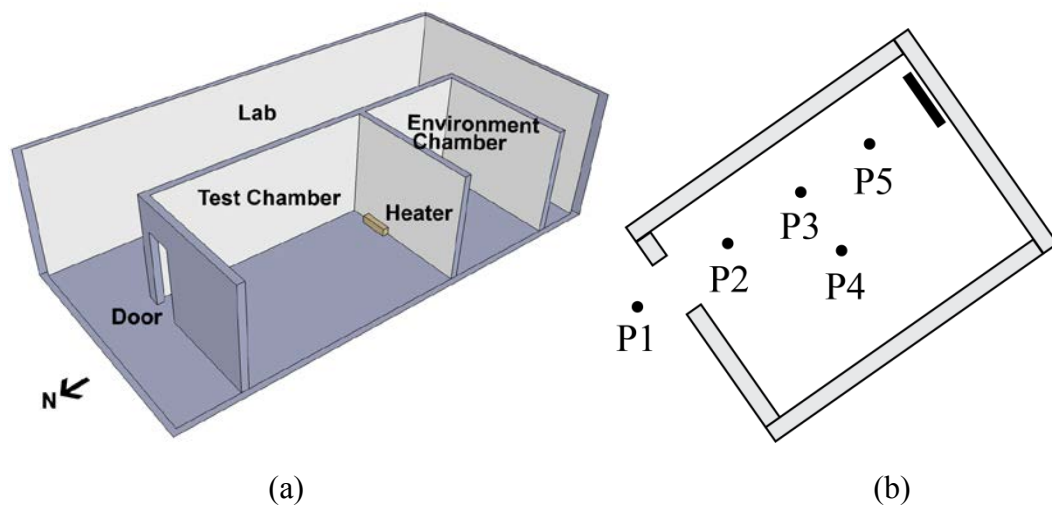
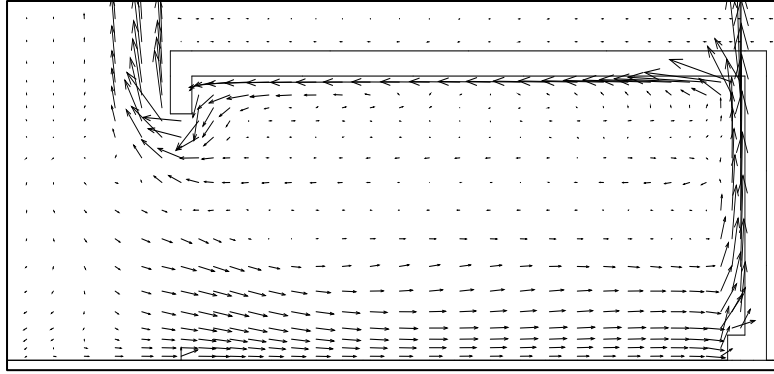
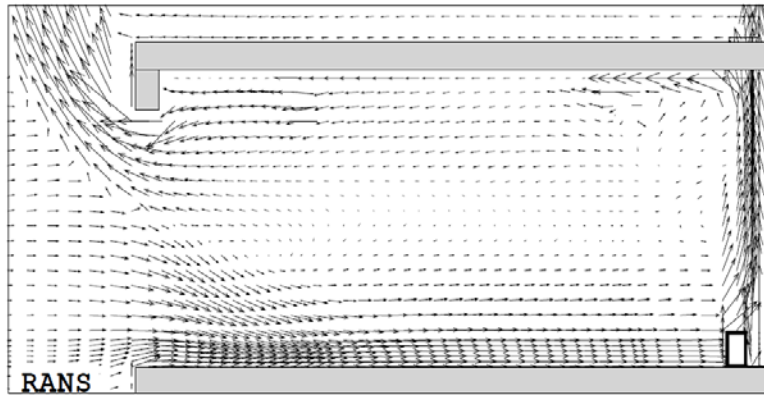


Figure 5



(a)



(b)

Figure 6

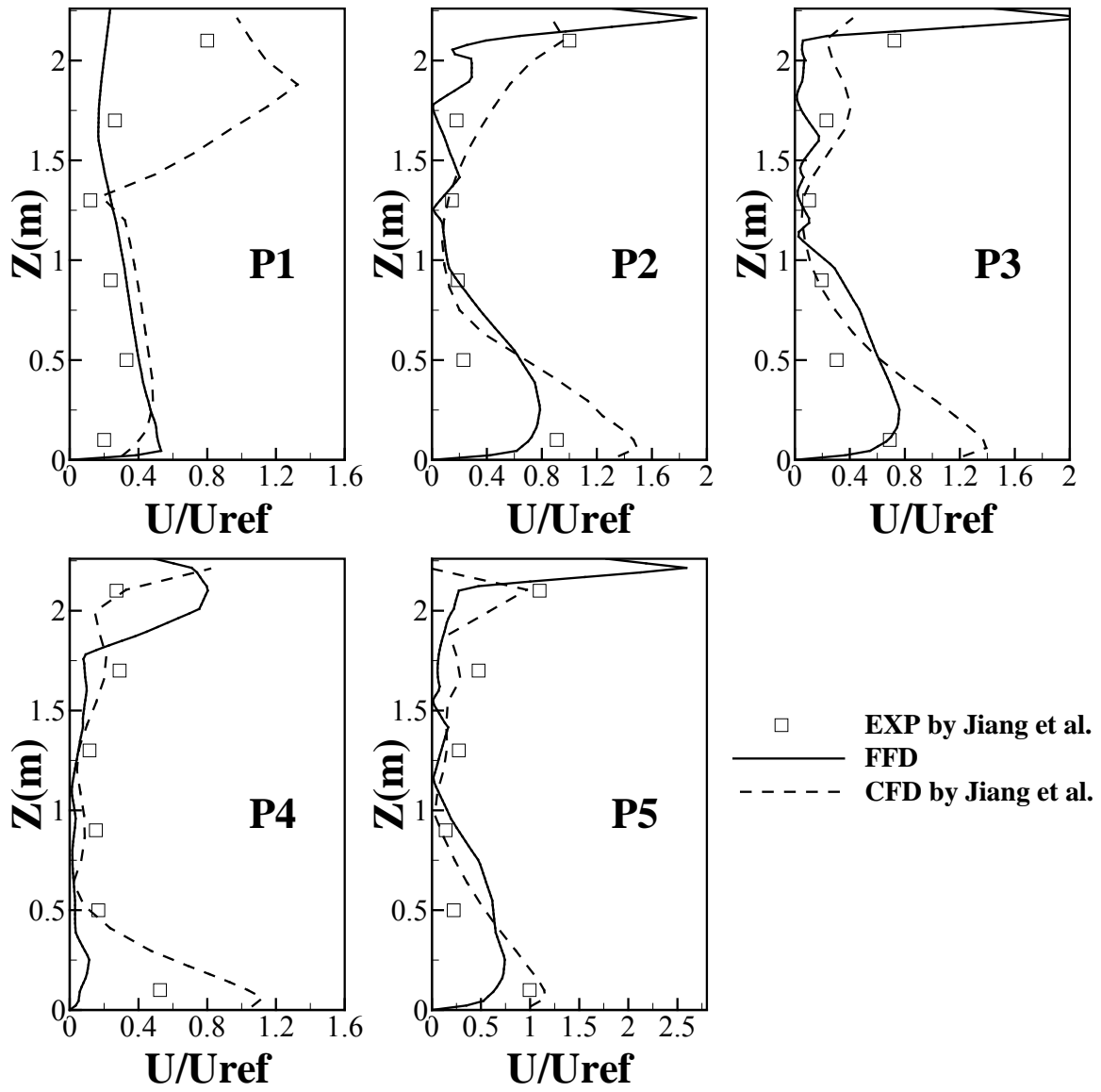


Figure 7

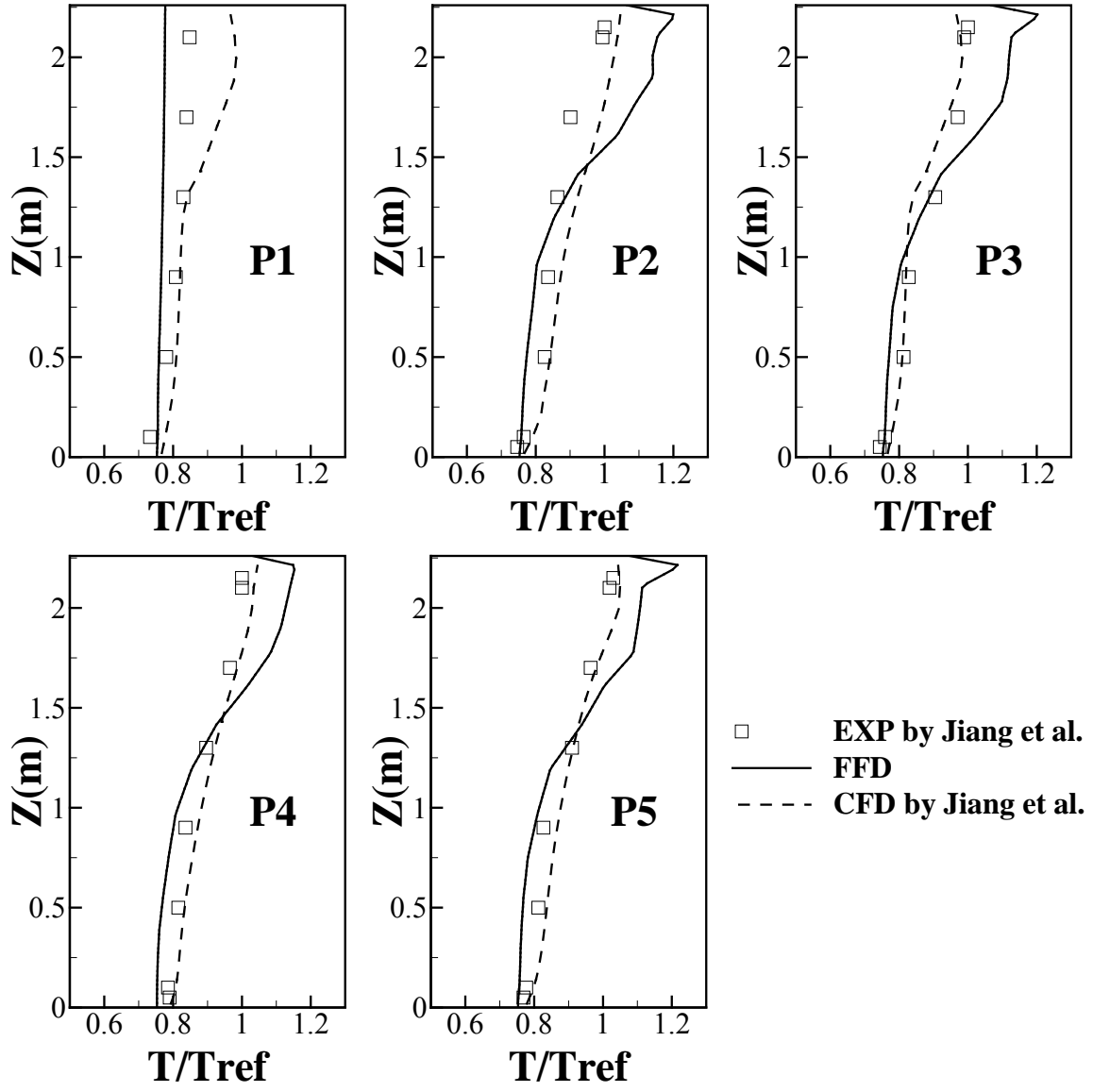


Figure 8

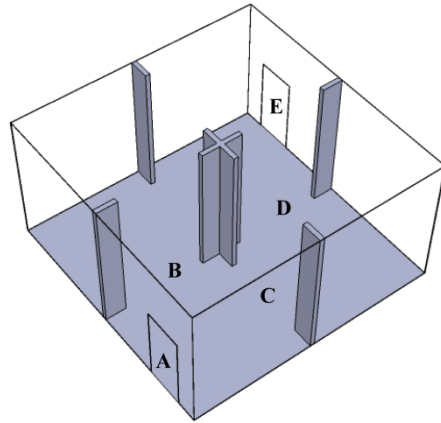
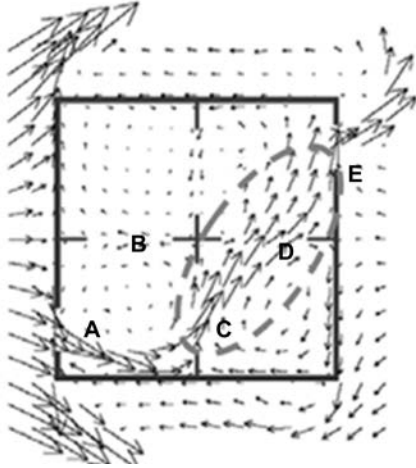
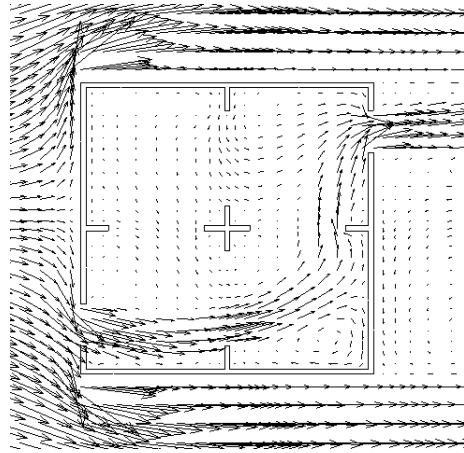


Figure 9



(a)



(b)

Figure 10

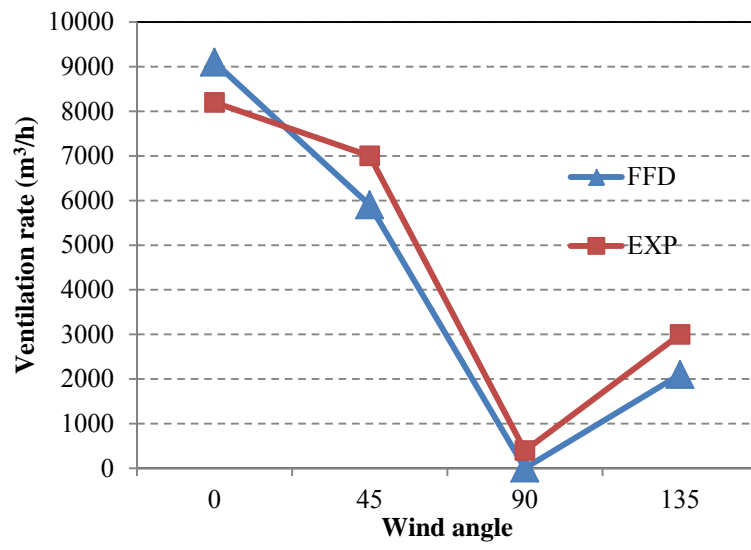


Figure 11

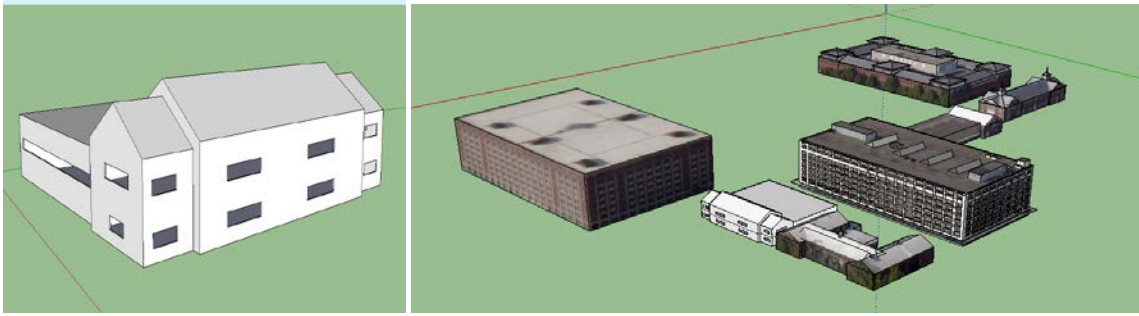


Figure 12

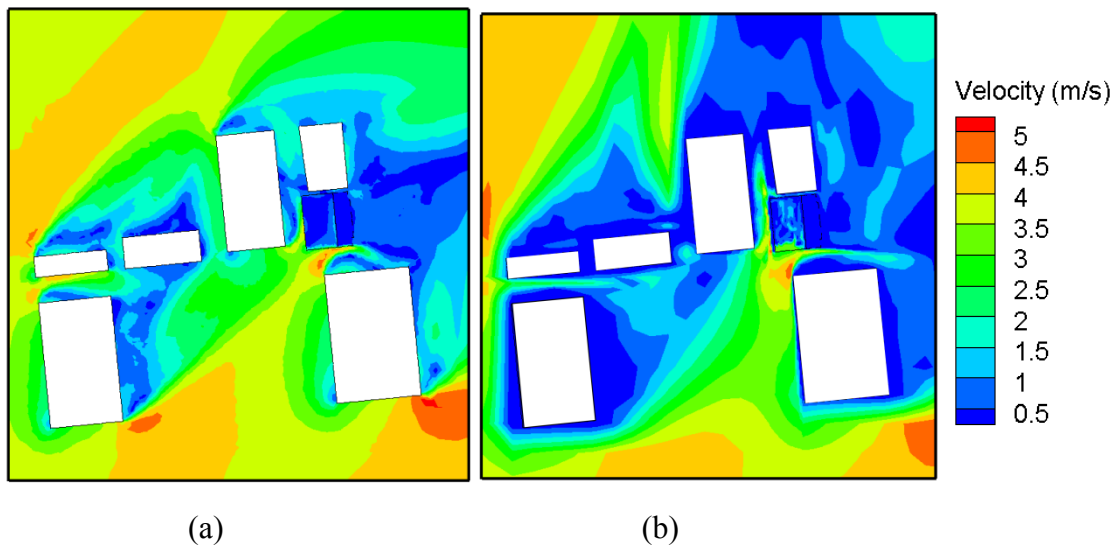


Figure 13